

1N-02
47946
P-20

Recent Improvements to and Validation of the One Dimensional NASA Wave Rotor Model

Daniel E. Paxson
National Aeronautics and Space Administration
Lewis Research Center
Cleveland, Ohio

and

Jack Wilson
NYMA Inc.
Engineering Services Division
Cleveland, Ohio

(NASA-TM-106913) RECENT
IMPROVEMENTS TO AND VALIDATION OF
THE ONE DIMENSIONAL NASA WAVE ROTOR
MODEL (NASA. Lewis Research
Center) 20 p

N95-2596.

Unclass

May 1995

G3/02 0047946



National Aeronautics and
Space Administration

8

8

RECENT IMPROVEMENTS TO
AND VALIDATION OF THE ONE DIMENSIONAL
NASA WAVE ROTOR MODEL

Daniel E. Paxson
NASA Lewis Research Center
Cleveland OH, 44135

Jack Wilson
NYMA

SUMMARY

A numerical model has been developed at the NASA Lewis Research Center which can predict both the unsteady flow quantities within a wave rotor passage and the steady averaged flows in the ports. The model is based on the assumptions of one-dimensional, unsteady, perfect gas flow. The model assesses not only the dominant wave behavior, but the loss effects of finite passage opening time, leakage from the passage ends, viscosity, and heat transfer to and from the passages. The model operates in the rotor reference frame; however, until recently no account was made for the often significant effect of the rotor circumferential velocity component. The present model accounts for this by modifying the passage boundary conditions, allowing the internal computational scheme to remain in the rotor reference frame, while quantities such as inlet duct stagnation properties may be specified in the fixed or absolute reference frame. Accurate modeling of this effect is critical to successful wave rotor analysis and design, particularly in off-design predictions where the flows in the inlet ducts are mis-matched with the rotor passages and significant turning may take place (i.e. work is done on the gas). The relative simplicity of the model makes it useful for design and optimization, as well as analysis, of wave rotor cycles for many applications. This report, building on several earlier papers, will describe the most recent modifications to the model. These include accounting for the relative/absolute transition at the passage boundaries, and refinements to the viscous source term correlation which resulted from this accounting. Comparison of model predictions with measured data will then be presented and discussed.

1.0 INTRODUCTION

The performance of wave rotors has often been modeled using inviscid compressible gasdynamic theory or unsteady acoustic theory. It is also usually assumed that the passage ends open and close instantaneously as they enter and exit the various ports (i.e. a shock tube diaphragm), and that the circumferential velocity of the rotor is small in comparison with the axial velocities. Experience has shown however, that predictions based on these assumptions do not agree with experimental measurements^{1,2,3}. The reason seems to be that the so called secondary effects and losses can have a tremendous impact on the wave rotor performance. These losses include, but are not limited to⁴, viscosity, leakage to and from the passage ends, finite passage

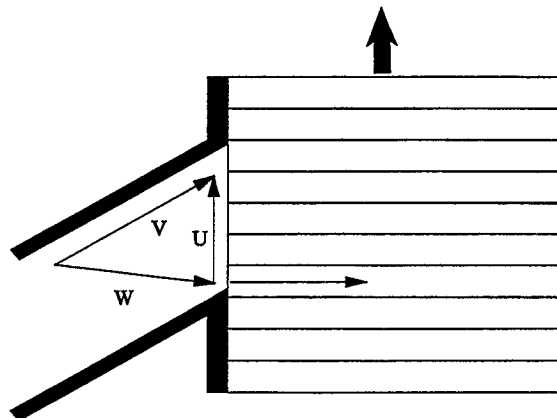


Figure 1 Wave rotor inlet duct

opening time, and mixing losses in the ports^{5,6,7,8}. Neglecting the circumferential component of velocity due to passage rotation can also lead to large miscalculations in performance. This is partly because neglecting this velocity component leads to improper calculation of boundary static properties, and partly because, in off design conditions, the flow in the ports is not aligned with the rotor passages and must be turned by the passage walls (see Figure 1). The turning leads to work addition or extraction from the flow, supplied by or to the drive motor. The work can be quite large and is always inefficient. A model which accurately predicts wave rotor performance must somehow account for these losses and effects. Two and three dimensional CFD models which include the rotor ducts in the computing domain have the flow turning built in; however, they are often either computationally expensive⁴, and/or neglect many other loss mechanisms⁹. This makes them impractical as preliminary design and full envelope analysis tools, at least for the present time. To this end, a relatively simple numerical model has been developed at the Lewis Research Center expressly for design and analysis of wave rotor cycles. The model solves the governing flow equations for a perfect gas in a hypothetical wave rotor passage with up to six ports using a high resolution, one-dimensional, explicit computational scheme with source terms. The source terms account for losses due to viscosity, heat transfer and leakage. The loss due to finite opening time, and the effect of flow turning, are incorporated into specialized boundary conditions. The mixing losses associated with non-uniform port flows are assessed after the passage traverses the ports.

Many of the details of this model have been presented in earlier reports^{1, 8, 10}. This report is intended as a supplement to them, and deals specifically with the two most recent modifications. In particular, it first describes the specialized boundary conditions which account for the shift from the absolute frame of reference where duct properties are specified to the rotor relative frame where the computational model operates. These include the effect of off design flow turning. Secondly, it will describe an update of the viscous source term^{8, 10} which is based on a semi-empirical correlation that has been refined using the now substantial experimental data from the NASA wave divider experiment¹¹. After presentation of these modeling improvements comparisons will be made between model predictions, and two experiments: the NASA wave rotor and a wave rotor built in the early 1960's by the Power Jets Company². Conclusion will then be drawn concerning the accuracy and generality of the model.

2.0 BOUNDARY CONDITIONS

The specification of appropriate boundary conditions for the wave rotor model is difficult, as it is with any system governed by hyperbolic equations. The problem arises because the type of information required at the boundaries depends on the direction of flow, but the direction of flow depends on the boundary conditions. As a result, the model must somehow anticipate what the direction of flow will be at the next instant of time based on information from the present time. This problem, and the author's solution, have been discussed in detail in reference 1. In that report however, there was no accounting for the circumferential velocity component of the rotor (i.e., it was assumed to be zero). In other words, the absolute and relative frame of reference were considered identical. For the case of outflow, where only the static pressure at the boundary is supplied, the two reference frames are interchangeable and thus, need not be discussed any further. For the case of inflow, the situation is quite different. Here, there are generally two pieces of information which must be supplied at the boundary. Those used in this model are the absolute stagnation pressure and temperature. Ultimately the model must use this stagnation state and whatever is known of the interior gas state at the present time to derive initial conditions for the image cells (computational cells just outside the computing domain) at the next time step. The best way to illustrate this idea is to simply describe the inflow boundary algorithm used in the model for both the fully and partially opened passage. It is noted that the algorithm is only valid for rotors in which the passages are straight and aligned with the axis of rotation.

2.1 Fully Open Passage Inflow

Consider Figure 2 which shows a portion of one passage including the first computational cell, the associated inlet duct flow, and the relevant nomenclature. The absolute stagnation pressure and temperature, and the duct angle β are prescribed. An initial guess is made for the pressure at the duct exit plane p_e . It is assumed that the flow in the duct is isentropic and steady. Therefore, if p_e is known, so are the exit plane velocity and density, u_e and ρ_e . Note that these quantities are in the absolute reference frame. The effective flow angle β_{eff} is also known by virtue of a relation to be described later. Suffice it to say that in most cases it is very close to the duct angle. Since the wheel speed is known ($U=\omega R$), simple vector addition yields the relative velocity W which, in general, is not aligned with the passage. To cross the duct exit plane and enter the passage the flow is assumed to go through some instantaneous turning process and emerge in the state denoted by the subscript 0 (the image cell). Although shown as finite in the figure, the space occupied by the image cell is assumed infinitesimal making the exit plane and left side of the first cell spatially coincident. A steady state balance of mass and energy through an infinitesimally thin control volume moving with the passage and containing the exit plane yields the equations

$$\rho_0 = \frac{\rho_e u_e \cos(\beta_{\text{eff}})}{u_0} \quad (1)$$

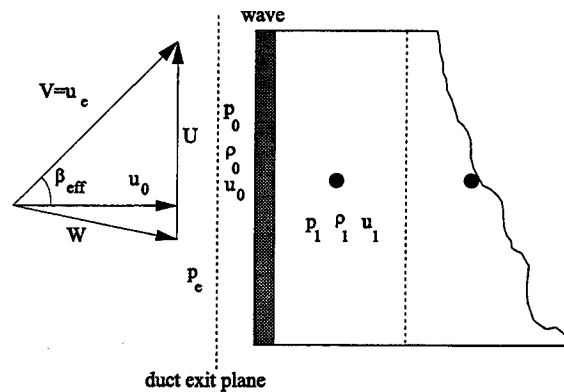
$$T_0 + \frac{u_0^2}{2c_p} = T_e + \frac{W^2}{2c_p} \quad (2)$$

or with $W^2 = (u_e \sin(\beta_{\text{eff}}) - \omega R)^2 + (u_e \cos(\beta_{\text{eff}}))^2$

$$T_0 = T_e + \frac{\omega R (\omega R - 2u_e \sin(\beta_{\text{eff}})) - u_0^2}{2c_p} \quad (3)$$

where T^0 is the stagnation temperature, ω is the rotor rotational speed, R is rotor radius, and c_p is the gas specific heat at constant pressure. A momentum balance yields no new information since, under the assumption of instantaneous turning, each momentum equation (x and y) contains an unknown body force. Instead, it is assumed that the relative velocity component which is aligned with the passage passes through undisturbed and that the perpendicular component is completely lost¹², i.e.

$$u_0 = u_e \cos(\beta_{\text{eff}}) \quad (4)$$



Equations 1, 3, and 4 allow ρ_0 , u_0 , and T_0 to be obtained directly from the known exit state and duct angle. The pressure p_0 is then obtained from the ideal gas law. In general, p_0 , ρ_0 , and u_0 will not match p_1 , ρ_1 ,

Figure 2 Fully open duct flow and passage

and u_1 (from the previous time step). This gives rise to some type of wave and contact discontinuity separating the two regions. If the normal shock or isentropic fan relations¹³ are used (depending on the pressure ratio across the wave system) with the quantities p_0 , p_1 , ρ_1 , and u_1 then a new quantity, u_0^* may be obtained. If u_0^* matches u_0 found using equation 3 then p_e was guessed correctly. If not then a new guess at p_e may be made using a numerical root finding technique¹⁴ on the function $y(p_e)=u_0-u_0^*=0$. This process may be repeated iteratively until $|y|$ is less than some specified tolerance. When this occurs the computational scheme proceeds to the next time step. A good initial guess for the exit pressure p_e may be found in appendix 1. The value for the effective flow angle β_{eff} is calculated using the following relation

$$\beta_{\text{eff}} = \beta - \left(\beta - \sin^{-1}(\text{arg}) \right) \left(\frac{p_e - p_e^{\text{sonic}}}{p^0 - p_e^{\text{sonic}}} \right)^6 \quad (5)$$

$$\text{arg} = \min \left(1.0, \frac{\omega R}{u_e} \right)$$

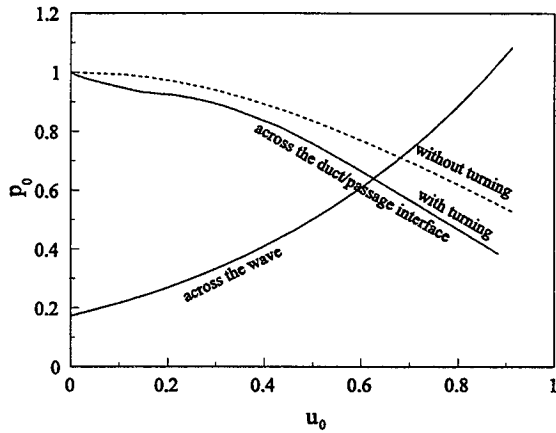


Figure 3 Boundary condition iteration.

where p^0 is the duct absolute stagnation pressure, and β is the duct angle. Equation 5, which was empirically developed by the author using experimental data from the NASA test rig and Reference 2, reflects the fact that in off design conditions the flow in the duct is turned to some degree before it enters the passage and furthermore, that the amount of turning in the duct depends on the incoming Mach number. Figure 3 graphically illustrates the iterative process described above. All of the flow quantities have been nondimensionalized by the duct stagnation state (the velocities by the stagnation speed of sound). The horizontal axis is the relative velocity in the image cell, u_0 . The vertical axis is the image cell pressure, p_0 . The case chosen is one where the flow in cell 1 is at a velocity, $u_1 = 0.5$ (relative to the passage) with a

pressure, $p_1 = 0.5$, and a density, $\rho_1=1.0$. The duct angle is 36 degrees and the wheel speed $U = 0.32$. The monotonically increasing curve represents the jump across the wave which separates the image and first cell. The solid decreasing curve represents the flow turning process between the duct and the passage image cell. The intersection of these two curves gives the correct value for p_0 and u_0 . The value used for p_0 is then found from equation 1. Also shown in the figure is the curve representing the flow process between the duct and passage if no turning effects are accounted for (i.e. the original model boundary conditions where $\beta = R = 0.0$). It can be seen that the turning process can substantially affect the converged image cell value and therefore the entire model behavior.

2.2 Partially Open Passage Inflow

For a partially open passage, the flow from the duct to the image cell is assumed to undergo two separate processes. As illustrated in Figure 4, the first process is the same turning action described by equations 1-4. After turning, the flow is then assumed to expand instantly from the partially opened area to the full passage area in a fictitious mixing zone. The mixing calculation has been described in detail in reference 10. The same iterative procedure described in appendix 1 is used here except the value of u_0 used in the function $y(p_e)$ is the image cell velocity calculated after the mixing zone. If the initial guess at this function $y(p_e^{\text{sonic}})$ does not yield a positive value then it is assumed that the flow is choked. The state of the flow after the turning process becomes frozen and, as described in reference 10, the iteration process changes. The mass and energy flux entering the mixing zone control volume are now fixed. As a result, if p_0 is specified, u_0 may be calculated, as can u_0^* . Thus, the choked flow iteration uses the image cell pressure as the independent variable instead of the duct exit pressure.

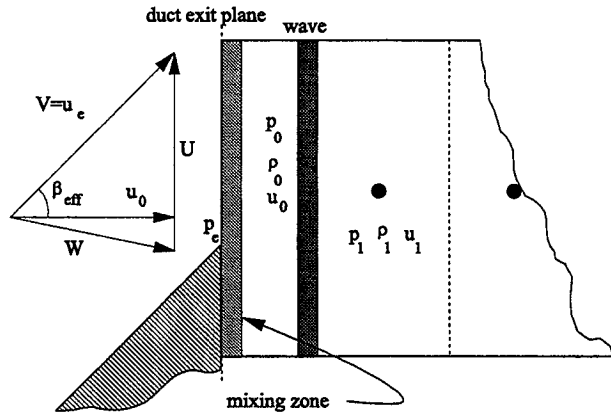


Figure 4 Partially open inflow duct and passage

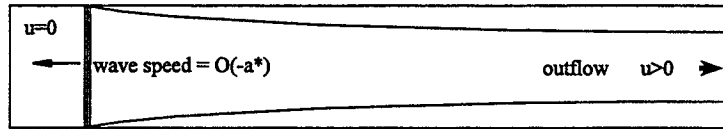
As described in reference 10, the effect of fluid viscosity in a one dimensional model is manifested primarily as shear stress on the passage walls. The wall shear stress is represented in the governing Euler equations as a source term in the momentum balance. Using the skin friction coefficient, c_f , the source term may be written as

3.0 VISCOUS SOURCE TERM

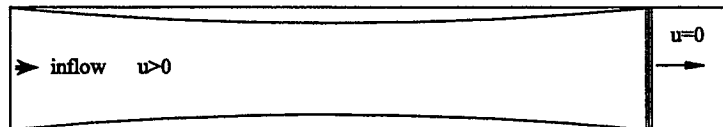
As described in reference 10, the effect of fluid viscosity in a one dimensional model is manifested primarily as shear stress on the passage walls. The wall shear stress is represented in the governing Euler equations as a source term in the momentum balance. Using the skin friction coefficient, c_f , the source term may be written as

$$s_2 = 2 \frac{c_f}{D_h} \rho u^2$$

$$c_f = \frac{\tau_{\text{wall}}}{\frac{1}{2} \rho u^2} \quad (6)$$



a) boundary layer growth behind an expansion fan



b) boundary layer growth behind a shock in an inlet region

Figure 5 Boundary layer growth

where D_h is the passage hydraulic diameter. The skin friction coefficient is assumed to depend on the passage geometry and the local Reynolds number. In particular, the relationship used in the present model is

$$c_f = \alpha (Re_\delta)^{-n} \left(\frac{\delta}{D_h} \right)^y \left(\frac{L}{D_h} \right)^z$$

$$\delta = \sqrt{\frac{v^* L}{a^*}}$$
(7)

where α is a constant, L is the passage length, and a^* and v^* are a reference speed of sound and kinematic viscosity respectively. The dynamic viscosity, μ is assumed constant. Equation 7 combines several interpretations of the nature of the boundary layer in a wave rotor passage. These are illustrated in Figure 5. The first two terms alone, α and $(Re_\delta)^{-n}$, may be derived from the solution to the flowfield around a flat plate passed over by a shock or expansion wave¹⁵, where the wave speed is represented by a^* (Figure 5a). The value of n in this case would be 0.5. The first, second, and third terms are an approximate solution to an incompressible flowfield in a pipe which is suddenly exposed to a pressure gradient¹⁵ for a time period equal to L/a^* . This solution accounts for the fact that the boundary layer may become thick in comparison with the passage hydraulic diameter. Finally, if $n=y=z=1/2$ then equation 7 is an approximate solution for steady, laminar, incompressible flow in the entry region of a pipe. This solution, illustrated in Figure 5b, accounts for the fact that in at least some portion of the wave rotor cycle, the passage boundary layer height may be restricted because it terminates both directly behind the initiating wave and at the passage leading edge.

If the governing momentum equation is normalized by the reference state p^* , ρ^* , and a^* and the reference time L/a^* , then equations 6 and 7 may be combined as

$$s_2' = \sigma_2 |\rho' u'|^{1-n} u'$$

$$\sigma_2 = 2\alpha \left(\frac{L}{D_h} \right)^{1+y+z} Re^{*\frac{-n+y}{2}}$$

$$Re^* = \frac{a^* L}{v^*}$$
(8)

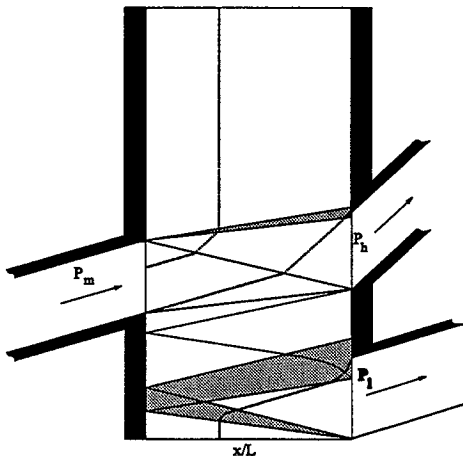


Figure 6 NASA rotor wave diagram

where the primes denote normalized quantities. The absolute value signs are used to insure that the viscous source term always opposes the motion. The values of α , n , y , and z in equation 8 were obtained using data from the NASA wave rotor divider experiment which has been described previously¹¹. The wave diagram and nomenclature are shown in Figure 6. The relevant geometry is listed in Table 1. Briefly, a wave divider accepts the working fluid through an inlet duct at some intermediate pressure P_m . It then splits the flow and delivers it through two exhaust ducts. In one of these the fluid is at a higher stagnation pressure P_h than the inlet flow, while in the other the pressure P_l is lower. The work addition to the high pressure flow and extraction from the low pressure flow is

achieved through the unsteady wave processes. The NASA experiment ran at a constant ratio of high pressure port to inlet mass flow, ξ of 0.37. The procedure for determining the unknowns of equation 9 was as follows. Two experimental runs were compared which had the same rotor geometry and inlet stagnation temperature but different stagnation pressures (30 vs. 10 psia). From the standpoint of equation 9, this meant that L/D_h , and Re^* remained constant. The experimentally measured boundary conditions (inlet stagnation pressure and temperature, and exit static pressures) corresponding to the highest mass flow point of each run were input to the model. The values of σ_2 and n were then adjusted until the same values for both computed cases produced the experimentally measured ξ . A value of $n=0.25$ produced the best result. The high mass flow point was used because this is where the experiment is designed to run. Thus, the flows are well aligned with the ducts and the turning calculation in the model is unused. This allowed the friction loss to be evaluated without having to simultaneously consider the effects of flow turning. Note that finite opening time effects are quite small in this experiment. Leakage effects are not small and cannot be evaluated independently from the viscous effects.

Configuration	Radius	Length	Passage Height	Number of Passages	Rotor Speed
Long/Wide	0.152	0.229 m	1.02 cm	65	3700 rpm
Long/Narrow	0.152	0.229	1.02	130	3700
Short/Wide	0.152	0.457	1.02	65	7400
Short/Narrow	0.152	0.457	1.02	130	7400

Table 1 NASA Rotor Configurations

With n determined, two more experimental runs were compared (also at the high mass flow points). One was the higher pressure inlet run described above, the other maintained the same inlet conditions, rotor speed, rotor length, and port positions but had a larger passage width (i.e. hydraulic diameter). This meant that Re^* remained the same but L/D_h was smaller. The boundary conditions for the wide passage run were then input to the model and the value of σ_2^{wide} adjusted until the computed and measured ξ matched. The value of σ_2^{narrow} was already known from the determination of n . From the definition of σ_2 in equation 8, it is found that

$$\frac{\ln\left(\frac{\sigma_2^{wide}}{\sigma_2^{narrow}}\right)}{\ln\left(\frac{D_h^{narrow}}{D_h^{wide}}\right)} = 1+y+z \quad (9)$$

The experiment was also run using a configuration in which the rotor was twice the length described above and ran at one half the speed. It also had the wide and narrow passage variations. Thus the process just described could be used with this rotor to establish another value for the quantity $1+y+z$. The final value used in the model is the average of the long and short rotor values and was found to be $1+y+z=1.081$.

After completing the comparisons (long, short, narrow, wide) four values for σ_2 had been obtained. Each of these was divided by the corresponding L/D_h raised to the 1.081 power. The natural log of the results were

then plotted versus the natural log of the corresponding Re'' 's. The best fit line through this plot determined the value of $(n+y)/2$ in equation 8. This was found to be 0.3953. The x-intercept determined the value of α which was found to be 2.724. Solving simultaneously for the exponents yielded: $y=0.5406$, and $z=-0.4596$.

4.0 RESULTS

There are two experiments with which the model has been extensively compared. The first was constructed by the Power Jets Corporation in the early 1960's and operated by J. A. C. Kentfield at the University of London². This experiment was designed such that the rotor could function as either a wave divider or equalizer cycle. An equalizer accepts a high pressure working fluid in one port and a low pressure fluid through another. The two flows are combined (e.g. work extracted from the high pressure flow and work done on the low pressure flow) and exit the rotor through an exhaust port at a common pressure and velocity. The second experiment to which has been compared is the NASA Lewis experiment described above and in Reference 11.

Divider and equalizer cycles are useful for wave rotor studies because they are relatively simple to construct and operate yet they demonstrate the governing principles and are subject to all of the major loss mechanisms. These two experiments are particularly useful for model validation because each emphasizes different losses and because each operates using a different wave diagram. The Power Jets rotor has wide passages, a low circumferential velocity and small gaps between the rotor and endwalls. This means that effects from friction and leakage are low but those from finite passage opening time are high. Furthermore, the ducts are aligned with the axis of rotation which therefore requires significant turning of the flow to get on board. All of the rotor configurations in the NASA experiment, on the other hand, have relatively narrow passages and large gaps between rotor and endwall. Thus, opening time effects are small and friction and leakage effects are high. The ducts for each of the NASA configurations are also angled such that, at the design point, the flow is well aligned with the rotor. This means that flow turning effects are only large at off design.

4.1 The Power Jets Experiment

The Power Jets rotor was 11 inches long, had a mean radius of 3.24 inches, a passage height of 2.2 inches, and contained 30 passages. For the data with which the model was compared, the rotational speeds were 6000 and 5500 r.p.m for the divider and equalizer configuration respectively. The gap between the rotor and endwalls was held to 0.007 inch. The low pressure port exited to the atmosphere through a flow meter for the divider configuration (in the model this port was held at constant atmospheric pressure) and accepted atmospheric air through a bell mouth in the equalizer. The divider inlet and high pressure ports, and the equalizer high pressure inlet and exhaust ports were equipped with valves for adjusting mass flow and port pressures. The divider inlet and equalizer high pressure inlet were maintained with a constant stagnation temperature of 555 R.

The nominal divider wave diagram is shown as an insert in Figure 7. The main plot in Figure 7 shows the high pressure port stagnation pressure versus low pressure port stagnation pressure for several families of constant ξ , where $\xi = \frac{\dot{m}_h}{\dot{m}_m}$. All pressures have been normalized by the inlet (medium) stagnation pressure. The lines represent experimental results while the open symbols (and asterixes) represent results from the model. The technique for obtaining port stagnation properties from the model calculation is described in Appendix 2. The predicted and measured results agree well over the entire operating regime of the wave rotor. The largest discrepancies occur for the $\xi=0.1$ curve where the model overpredicts the measured performance.

Also shown in Figure 7 are two curves representing experimental and computed lines of constant inlet Mach number which is an indirect measure of mass flow. The model inlet Mach number was found from the computed mass flow and the specified inlet stagnation temperature and pressure. The effect of blockage due to the thickness of the passage walls was accounted for by multiplying the computed mass flow by the ratio of passage width to passage width plus wall thickness. For the Power Jets experiment this ratio was 0.88. It is seen that the model consistently overpredicts the mass flow through the device. For this $M_m=0.3$ curve, the overprediction is approximately 11%. The reason for this is unknown;

however, it is noted that the same phenomenon has been observed in a two dimensional viscous CFD calculation for one operating point of this device¹⁷. This may indicate the presence of some three dimensional effects since the hub tip ratio for the power jets experiment was only 0.49. The discrepancy does not seem to occur with predictions of the NASA rotor to be shown below. The hub tip ratio for the NASA rotor is 0.94

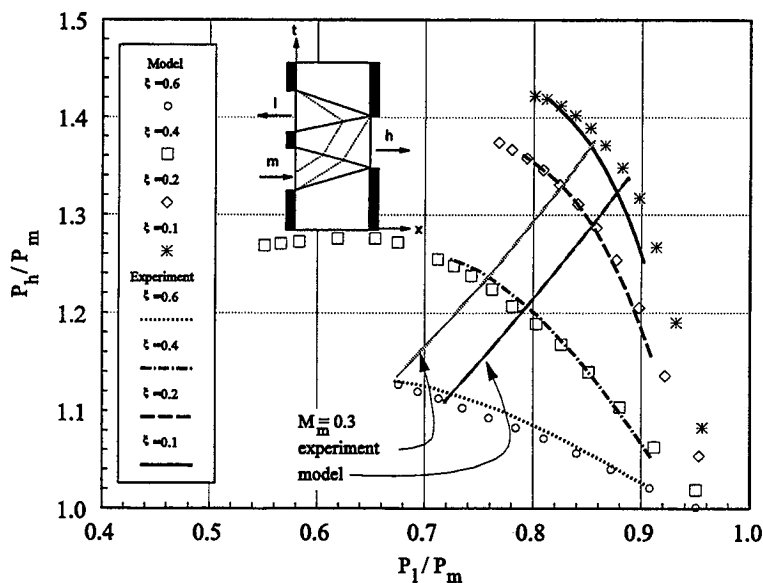


Figure 7 Power Jets wave divider

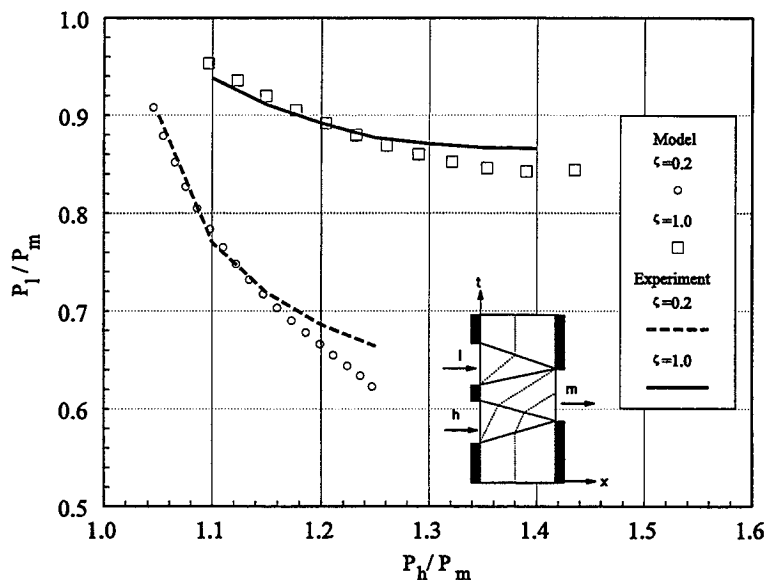


Figure 8 Power Jets wave equalizer

The measured and predicted equalizer performance curves are shown in Figure 8 along with the nominal wave diagram and port nomenclature. The curves represent lines of constant low pressure to high pressure port enthalpy flux ratio, $\zeta = \frac{\dot{m}_l T_l^0}{\dot{m}_h T_h^0}$.

The low pressure inlet stagnation temperature of the experiment was not stated in the reference and was thus assumed to be 520 R. The agreement between model and experiment is again generally good; however, discrepancies increase as the work transfer rate increases (moving rightward on the plot).

4.2 The NASA Lewis Experiment

Most of the details of this rotor were described in section 3.0. For the results to be presented, the inlet stagnation pressure and temperature were maintained at approximately 30 psia and 580 R respectively (except for the single low pressure test in which the inlet stagnation pressure was 10 psia). The leading wall of the inlet duct is rounded as shown in Figure 9. This creates a difficulty in modeling since the flow turning scheme assumes a constant duct angle. In order to proceed with the calculations, the profile shown in Figure 9 was assumed for the angle β in equation 5.

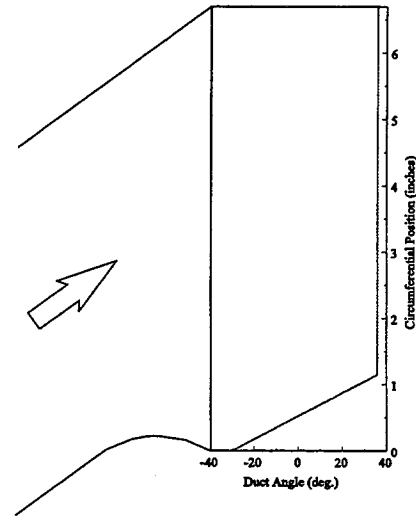


Figure 9 Assumed NASA rotor inlet β distribution

Figure 10 shows the computed (lines) and measured (symbols) high pressure port stagnation pressure versus low pressure port stagnation pressure for the constant $\xi=0.37$ used in the experiment. As with the Power Jets results, all pressures have been normalized by the inlet stagnation pressure. The experimental stagnation pressures shown were obtained using an average of the 4-5 stagnation probes distributed across, and aligned with, each duct. The model stagnation pressures were obtained using calculations described in Appendix 2. Each plot

represents a different rotor configuration which is labelled beside it. The expressions 'narrow' and 'wide' refer to the two passage widths listed in Table 1 while the expressions 'short' and 'long' refer to the two rotor lengths. The two curves in the 'short/narrow' plot represent the high and low inlet stagnation pressure tests described above. The model curves were obtained by fixing the inlet stagnation pressure, changing the low pressure exhaust static pressure to vary mass flow, and changing the high pressure exhaust static pressure to vary ξ .

Defining error as the ratio $e = \frac{(P_h)_{\text{experiment}} - (P_h)_{\text{model}}}{(P_h)_{\text{experiment}}}$, for a given P_l/P_m , the maximum value for all four

configurations is approximately 0.038 indicating good agreement between experiment and model. It is seen that the maximum errors occur with the wide rotor passage configuration. The reason for this is unknown. It is noted that all of the curves show a maximum which does not appear in the experimental data of the corresponding Power Jets plot (Figure 7). The Power Jets experiment was limited in mass flow by the compressor which supplied the wave rotor inlet. For this reason, the experimental curves in Figure 7 do not extend as far leftward as those in the NASA experiment. They can, of course, be extended by the model as shown for the $\xi=0.4$ curve, and when this is done, the same maxima are found.

It is interesting to examine the impact of the various modelled losses, and the relative/absolute and flow turning effects on the performance curve of Figure 10. This is done in Figure 11 for the short rotor with wide passages. Beginning with the loss free (except for shock and mixing losses) curve, this figure shows the performance as each successive loss mechanism is added to the model. Also shown in the figure for reference is the experimental performance curve. When examining this plot it should be kept in mind that each loss mechanism affects the speed of waves to some degree so that the mistiming of waves also becomes a factor in the shape of the various curves. It is noted that the rotor was actually designed using an early version of the model which accounted only for the finite opening time effects and for friction (with a considerably less refined correlation). Based on the model predictions it can be seen that, for this rotor, the dominant losses are incurred through friction and leakage. It is also observed that as one moves rightward on the plot, toward

decreasing mass flow, the work done on the gas through flow turning increases. This is reflected as a shift in the curve upward and to the right.

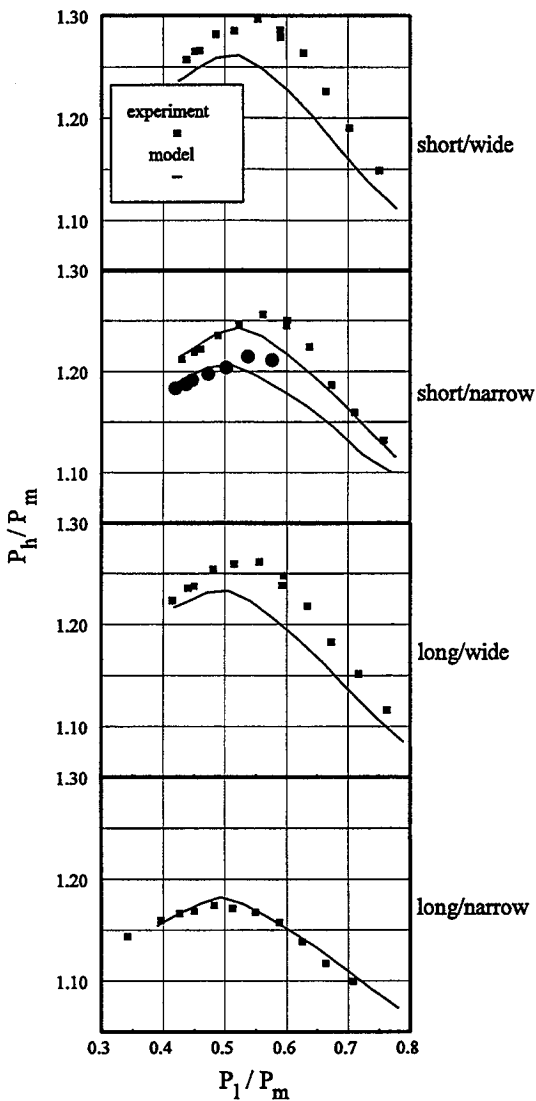


Figure 10 NASA rotor performance

divider and equalizer experiment, and with the NASA wave divider experiment. Favorable comparison was also found with experimental dynamic pressure traces and mass flow measurements on the NASA rotor. It was shown that, although wave rotor performance is dominated by unsteady gasdynamic waves, it is profoundly affected by the secondary losses described and analyzed in this, and previous reports. Further validation of the model is needed however, because the two experiments with which it has been compared so far were both relatively low mass flow rate machines (.5-5 lbm/s) and because neither experiment had large density or temperature changes. Wave rotors are presently envisioned for use as high pressure and temperature cores for gas turbine engines^{18,19}. In this capacity they will necessarily see higher flow rates (5-40 lbm/s) and large changes in density and temperature due to the use of an external combustor in the cycle. Large changes

Figure 12 shows the predicted and experimental mass flows versus the ratio of the low pressure port stagnation pressure to inlet port stagnation pressure for the various configurations of the NASA rotor. The same correction for the passage wall thickness described in section 5.1 was used here. The agreement is good and is particularly encouraging considering that none of the various parameters in the loss equations were correlated to the mass flow.

Finally, Figures 13, 14, and 15 show comparisons between predicted and experimental unsteady pressure traces on board a rotor passage as it rotates through a cycle for 3 different points on the performance curve of Figure 11 (the short/narrow configuration). The pressure has been normalized in these figures by the reference pressure of 30.25 psia. The locations of the transducers are shown as dashed lines on the inserted wave diagram of Figure 13. For reference, these locations are 0.45 inches from the passage ends. The location of the three points on the performance curve are shown as a second insert in Figure 13. The agreement is again good, even in the far off design point represented by Figure 15. It is noted that the intensity of the pressure spikes in Figures 13-15 is always higher in the model than in the experimental measurements. It is not known whether this discrepancy arises from errors in the model or from limitations in the transducer electronics.

5.0 CONCLUDING REMARKS

The wave rotor model described above has been successfully validated by demonstrating favorable performance comparisons with the Power Jets wave

in temperature give rise to changes in gas properties which cannot be accounted for with the calorically perfect gas assumption of the model. Large density changes give rise to large contact discontinuities in the wave rotor. These are abrupt (in the axial direction) jumps in density across which the pressure and velocity remain constant. These may be unstable in the presence of finite opening time effects⁵, reflected shock waves⁴, or high rotational speeds⁶, and quickly break down into highly two and three dimensional structures well beyond the capabilities of a one dimensional model. An experimental wave rotor which utilizes the type of cycle envisioned for the gas turbine core is presently being designed using the model and is scheduled for construction and testing at the NASA Lewis Research Center. The outcome of this experiment would be useful in answering some questions regarding the model capability.

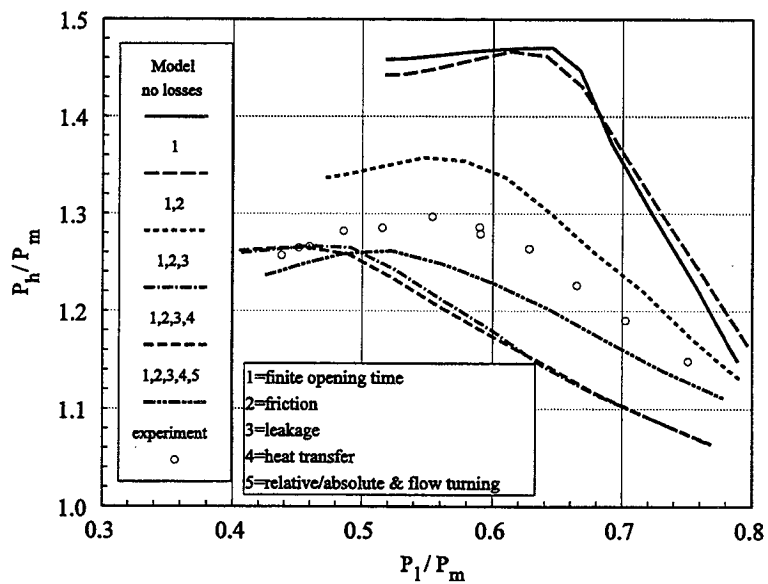


Figure 11 Performance effects from losses

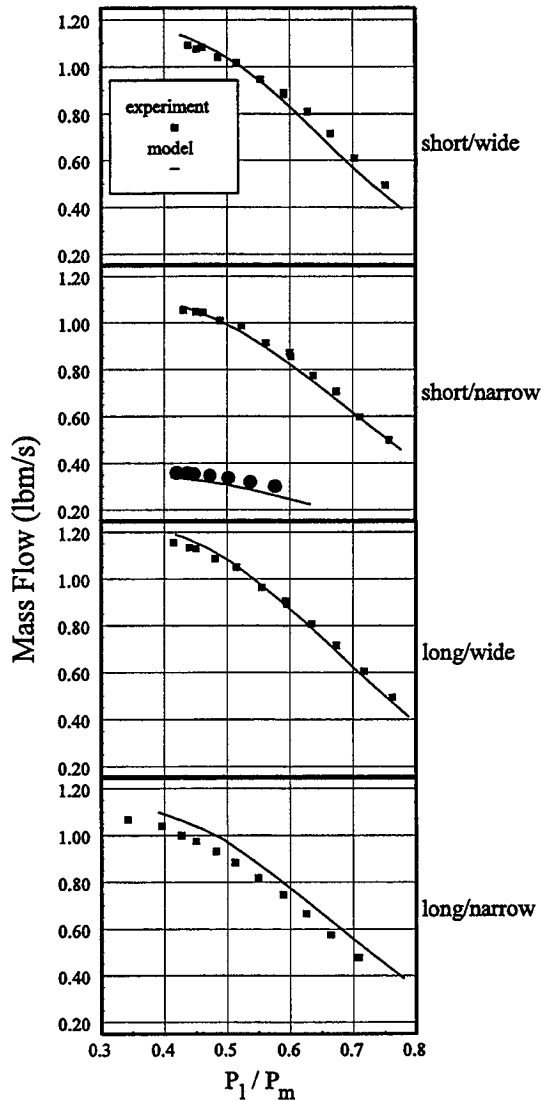


Figure 12 NASA rotor mass flow

REFERENCES

1. Paxson, D. E. , "A General Numerical Model for Wave Rotor Analysis", NASA TM 105740, 1992.
2. Kentfield, J. A. C., "An Examination of the Performance of Pressure-Exchanger Equalizers and Dividers", PhD Thesis, U. of London, 1963 (also in Journal of Basic Engineering, September, 1969).
3. Klapproth, J. F., "Wave Engine Project", General Electric Quarterly Reports, 1960.
4. Welch, Gerard, "Two-dimensional Numerical Study of Wave Rotor Flow Dynamics", Presented at the 29th Joint Propulsion Conference, Monterey, CA, 1993, paper # AIAA 93-2525.
5. Eidelman, S., "The Problem of Gradual Opening in Wave Rotor Passages", Journal of Propulsion, 1985, Vol. 1, No. 1, pp 23-27.
6. Larosiliere, L., Three Dimensional Numerical Simulation of Gradual Opening in a Wave Rotor Passage", Presented at the 29th Joint Propulsion Conference, Monterey, CA, 1993, paper # AIAA 93-2526.
7. Taussig, R. T., "Energy Exchanger Performance and Power Cycle Evaluation-Experiments and Analysis", Final Report DOE/ER/01084--T1, 1980.
8. Paxson, D. E., "A Comparison Between Numerically Modelled and Experimentally Measured Loss Mechanisms in Wave Rotors", Presented at the 29th Joint Propulsion Conference, Monterey, CA, 1993, paper # AIAA 93-2522.
9. Lear, W., and Candler, G. "Direct Boundary Value Solution of Wave Rotor Flow Fields", Presented at the 31st Aerospace Sciences Meeting, Reno, NV, 1993, paper # AIAA-93-0483.
10. Paxson, D. E., "An Improved Numerical Model for Wave Rotor Design and Analysis", presented at The 31st Annual Aerospace Sciences Meeting, Reno, NV, paper #AIAA-93-0482, 1993, also NASA TM 105740, 1993.

11. Wilson, Jack and Fronek, Dennis, "Initial Results From the NASA-Lewis Wave Rotor Experiment", Presented at the 29th Joint Propulsion Conference, Monterey, CA, 1993, paper # AIAA 93-2521.
12. Glassman, Arthur, J., "Turbine Design and Application", Volume 2, NASA SP-290, 1973
13. Anderson, John, D., Modern Compressible Flow, McGraw-Hill Book Co., 1982
Press, William, H. et. al., Numerical Recipes, Cambridge University Press, 1986.
15. Schlichting, Herman, Boundary Layer Theory, 7th edition, McGraw-Hill Book Co., 1979
16. White, Frank, M., Viscous Fluid Flow, McGraw-Hill Book Co., 1974
17. Welch, Gerard, personal consultation, January, 1995, also see reference 4.
18. Taussig, R. T., "Wave Rotor Turbofan Engines for Aircraft," Presented at The ASME Winter Annual Meeting, New Orleans, LA, 1984.
19. Wilson, Jack, and Paxson, D. E., "Jet Engine Performance Enhancement Through the Use of a Wave-Rotor Topping Cycle," NASA TM 4486, 1993.

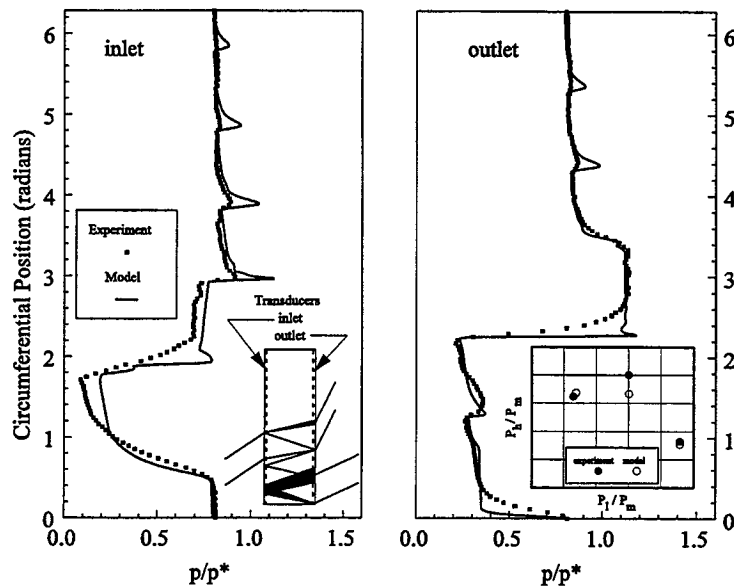


Figure 13 High mass flow pressure trace

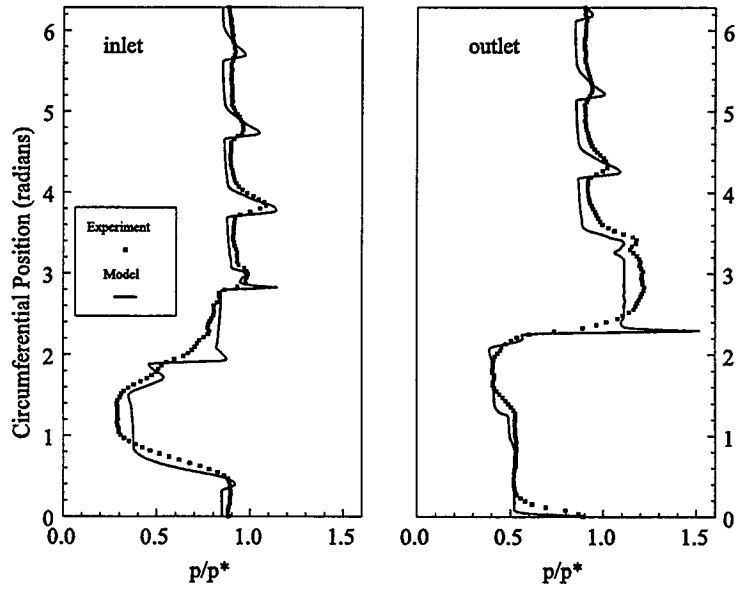


Figure 14 Medium mass flow pressure trace

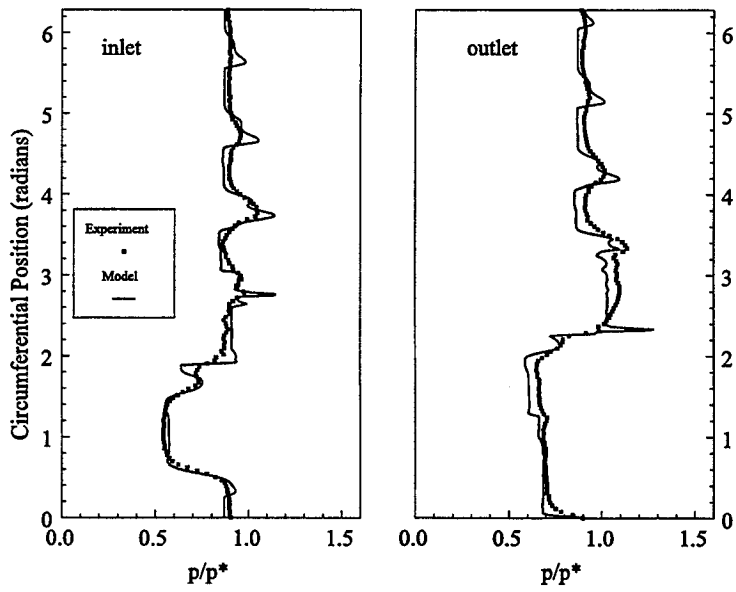


Figure 15 Low mass flow pressure trace

Appendix 1 Initial Guess for Root Finding Technique

Any numerical root finding technique requires an initial guess for the dependent variable (p_e). A good value for the procedure described in section 2.1 is to use the value which results in the flow being sonic in the image cell. Equations 1,2, and 3 may be rearranged to yield the following quadratic in u_e

$$\left[\left(Ma_0^2 \frac{\gamma-1}{2} + 1 \right) \cos^2(\beta_{eff}) \right] u_e^2 + \left[Ma_0^2 (\gamma-1) \omega R \sin(\beta_{eff}) \right] u_e - Ma_0^2 \left[\frac{\gamma-1}{2} (\omega R)^2 + (a^0)^2 \right] = 0 \quad (10)$$

where the duct stagnation speed of sound $a^0 = \sqrt{\gamma R T^0}$, γ is the ratio of specific heats, R is the real gas constant, and Ma_0 is the image cell Mach number. Setting $Ma_0 = 1.0$ and solving equation 10 for the positive value of u_e gives the absolute duct exit velocity which will yield a sonic velocity after turning. Since the duct flow is assumed isentropic and steady, the duct exit pressure p_e^{sonic} can then easily be calculated. If p_e^{sonic} does not yield a positive value of $y(p_e^{sonic})$ for the initial guess then it is assumed that the incoming flow is fully supersonic. In that case, additional information is required at the boundary since all of the image cell information must now be externally specified and none may be extracted from the interior of the computing domain. For this model this means that the image cell Mach number Ma_0 must be supplied. With Ma_0 specified and the duct stagnation Temperature and pressure, equations 1, 3, and 15 may be used to completely specify the image cell state. The effective angle is set equal to the duct angle since equation 4 would otherwise yield streamlines angled in the wrong direction. In extreme cases (large β_{eff} , or large wheel speed) equation 15 will lead to a negative duct exit pressure. If this happens, the initial guess for p_e is set to 0. If this does not yield a positive value of $y(p_e)$ then the program stops.

Appendix 2 Outlet Port Flows

Although the gasdynamics in the passages are interesting, it is ultimately some average value of the outlet port stagnation properties by which wave rotor performance is measured. In order to obtain these in the model a constant area mixing calculation is used. The calculation, described in reference 1 and detailed below, uses the time integrated mass momentum and energy flux from the passage over the period during which it is exposed to an outflow port. It is performed in the reference frame of the passage and results in a uniform, mixed static state which is representative of the flow some distance downstream if the wheel speed were low in comparison to the axial velocity component. The equations for the mixing calculation may be written as

$$\begin{aligned} \bar{u} &= \frac{\gamma \phi_{mo} - \sqrt{(\gamma \phi_{mo})^2 - 2(\gamma+1)(\gamma-1)\phi_e \phi_m}}{(\gamma+1)\phi_m} \\ \bar{p} &= \frac{\phi_m}{\bar{u}} \\ \bar{p} &= \phi_{mo} - \phi_m \bar{u} \end{aligned} \quad (11)$$

where

$$\begin{aligned}\phi_m &\equiv \frac{1}{\Delta\theta} \int_{\theta_1}^{\theta_2} \rho_0 u_0 d\theta = \bar{\rho} \bar{u} \\ \phi_{m_0} &\equiv \frac{1}{\Delta\theta} \left[\int_{\theta_1}^{\theta_1+\theta_p} (p_e + \rho_e u_e^2) \frac{A_e}{A_p} d\theta + \int_{\theta_1+\theta_p}^{\theta_2} (p_0 + \rho_0 u_0^2) d\theta + \int_{\theta_2}^{\theta_2+\theta_p} (p_e + \rho_e u_e^2) \frac{A_e}{A_p} d\theta \right] = \bar{p} + \phi_m \bar{u} \quad (12) \\ \phi_e &\equiv \frac{1}{\Delta\theta} \int_{\theta_1}^{\theta_2} \rho_0 u_0 \left(c_p T_0 + \frac{u_0^2}{2} \right) d\theta = \frac{\gamma}{\gamma-1} \bar{u} \bar{p} + \frac{\phi_m \bar{u}^2}{2}\end{aligned}$$

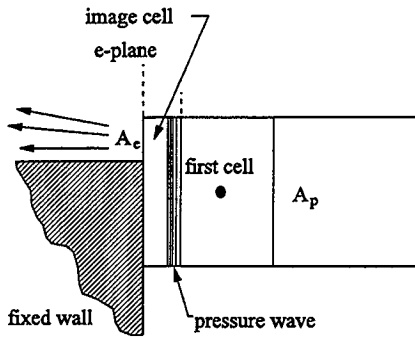


Figure 16 Partially opened passage-outflow

Here, the subscript 0 refers to the image cell adjacent to the port. The subscript e in the expression for ϕ_{m_0} refers to a fictitious exit plane of the image cell when the passage is partially open (see Figure 16 and reference 10). The ratio of A_e to A_p is that of the passage area exposed to the port to the fully open area. The angles θ_1 and θ_2 refer to circumferential position of the port opening and closing, θ_p refers to the circumferential extent of a passage, and $\Delta\theta$ is the circumferential extent of the port. Equation 12 is actually three equations with three unknowns which can be solved simultaneously to yield a quadratic in \bar{u} . The solution to the quadratic is the first line of equation 11

For comparison with the NASA wave rotor experiment the following isentropic relations are used to obtain absolute stagnation quantities (which are common performance indicators) from the mixed, relative quantities of equation 11

$$\begin{aligned}T^0 &= \frac{1}{c_p} \left(\frac{\phi_e}{\phi_m} + \frac{(\omega R)^2}{2} \right) \\ P^0 &= \bar{p} \left(\frac{T^0}{\bar{T}} \right)^{\frac{\gamma}{\gamma-1}}\end{aligned} \quad (13)$$

These relations assume that there are no losses associated with turning the flow if it is not aligned with the exit duct. This is obviously untrue; however, in the NASA experiment the total property probes in the ducts are located quite close to the rotor exit plane where little turning has taken place. Since stagnation probes are generally insensitive to incidence they will measure the absolute properties regardless of whether or not the flow is aligned with them. Furthermore, since there are several circumferentially distributed probes in a duct, and very little mixing has taken place in the exit plane, there is may be significant variation in measurements between probes. This is particularly true in off design situations. In order to account for this variation, a simple average is used; which is really a form of mixing calculation. Thus, the experimental procedure finds distributed absolute properties and averages them while the model averages the variations using equation 11 and then finds the total properties using equation 13.

In the Power Jets Experiment the stagnation properties were not measured directly but were calculated using

the known mass flow, and averaged static temperature and pressure measurements from probes in the duct near the rotor exit plane. Since the ducts were aligned with the rotor axis of rotation this technique did not account for the kinetic energy contributed by the circumferential velocity of the flow in the exhaust ports. In other words, the stagnation pressure obtained was measured in the relative frame of reference. As such, the model predictions in Figure 7 are presented in a similar manner, namely, equation 13 is used with $\omega R=0.0$ (Note that this applies only to exhaust ports, the inlet stagnation properties are specified). For comparison, the predicted absolute stagnation pressures are presented in comparison with the experimental results in Figure 17.

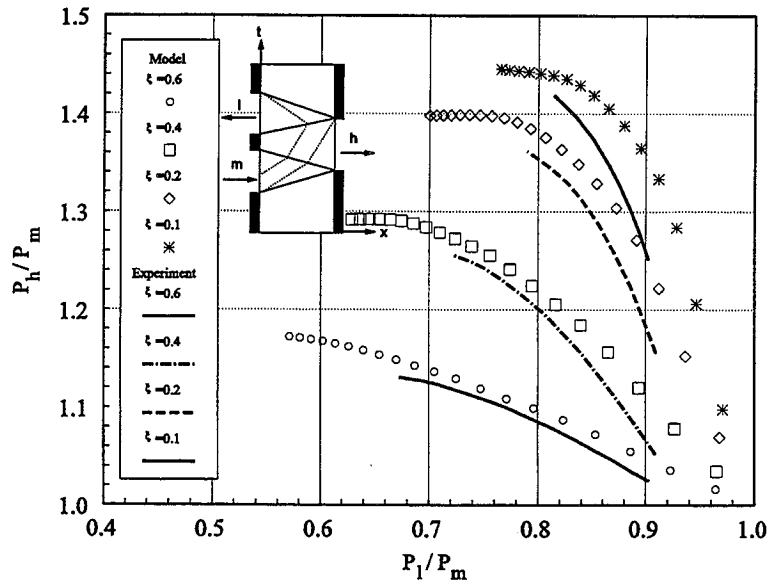


Figure 17 Power Jets wave divider absolute reference frame performance

REPORT DOCUMENTATION PAGE

Form Approved
OMB No. 0704-0188

Public reporting burden for this collection of information is estimated to average 1 hour per response, including the time for reviewing instructions, searching existing data sources, gathering and maintaining the data needed, and completing and reviewing the collection of information. Send comments regarding this burden estimate or any other aspect of this collection of information, including suggestions for reducing this burden, to Washington Headquarters Services, Directorate for Information Operations and Reports, 1215 Jefferson Davis Highway, Suite 1204, Arlington, VA 22202-4302, and to the Office of Management and Budget, Paperwork Reduction Project (0704-0188), Washington, DC 20503.

1. AGENCY USE ONLY (Leave blank)		2. REPORT DATE May 1995	3. REPORT TYPE AND DATES COVERED Technical Memorandum	
4. TITLE AND SUBTITLE Recent Improvements to and Validation of the One Dimensional NASA Wave Rotor Model			5. FUNDING NUMBERS WU-505-62-50	
6. AUTHOR(S) Daniel E. Paxson and Jack Wilson				
7. PERFORMING ORGANIZATION NAME(S) AND ADDRESS(ES) National Aeronautics and Space Administration Lewis Research Center Cleveland, Ohio 44135-3191			8. PERFORMING ORGANIZATION REPORT NUMBER E-9621	
9. SPONSORING/MONITORING AGENCY NAME(S) AND ADDRESS(ES) National Aeronautics and Space Administration Washington, D.C. 20546-0001			10. SPONSORING/MONITORING AGENCY REPORT NUMBER NASA TM-106913	
11. SUPPLEMENTARY NOTES Daniel E. Paxson, NASA Lewis Research Center and Jack Wilson, NYMA, Inc., Engineering Services Division, 2001 Aerospace Parkway, Brook Park, Ohio 44142 (work funded by NASA Contract NAS3-25266). Responsible person, Daniel E. Paxson, organization code 2560, (216) 433-8334.				
12a. DISTRIBUTION/AVAILABILITY STATEMENT Unclassified - Unlimited Subject Categories 07 and 02 This publication is available from the NASA Center for Aerospace Information, (301) 621-0390.			12b. DISTRIBUTION CODE	
13. ABSTRACT (Maximum 200 words) A numerical model has been developed at the NASA Lewis Research Center which can predict both the unsteady flow quantities within a wave rotor passage and the steady averaged flows in the ports. The model is based on the assumptions of one-dimensional, unsteady, perfect gas flow. The model assesses not only the dominant wave behavior, but the loss effects of finite passage opening time, leakage from the passage ends, viscosity, and heat transfer to and from the passages. The model operates in the rotor reference frame; however, until recently no account was made for the often significant effect of the rotor circumferential velocity component. The present model accounts for this by modifying the passage boundary conditions, allowing the internal computational scheme to remain in the rotor reference frame, while quantities such as inlet duct stagnation properties may be specified in the fixed or absolute reference frame. Accurate modeling of this effect is critical to successful wave rotor analysis and design, particularly in off-design predictions where the flows in the inlet ducts are mis-matched with the rotor passages and significant turning may take place (i.e. work is done on the gas). The relative simplicity of the model makes it useful for design and optimization, as well as analysis, of wave rotor cycles for many applications. This report, building on several earlier papers, will describe the most recent modifications to the model. These include accounting for the relative/absolute transition at the passage boundaries, and refinements to the viscous source term correlation which resulted from this accounting. Comparison of model predictions with measured data will then be presented and discussed.				
14. SUBJECT TERMS Wave rotor; CFD; Numerical simulation			15. NUMBER OF PAGES 20	
			16. PRICE CODE A03	
17. SECURITY CLASSIFICATION OF REPORT Unclassified	18. SECURITY CLASSIFICATION OF THIS PAGE Unclassified	19. SECURITY CLASSIFICATION OF ABSTRACT Unclassified	20. LIMITATION OF ABSTRACT	

